Available online at www.CivileJournal.org

Civil Engineering Journal

Vol. 5, No. 1, January, 2019

Investigation of k-ε Turbulent Models and Their Effects on Offset Jet Flow Simulation

Mohammad Reza Boroomand [a*], Amirhossein Mohammadi [a]

[a] *Department of civil Engineering, Tafresh University, Tafresh 39518 79611, Iran.*

Received 01 October 2018; Accepted 28 December 2018

Abstract

In the case in which relatively low thickness and high-velocity flow enter into the lower velocity fluid, the resulting interference field of these two flows is called the jet. This phenomenon is the dominant output of power plants and some of the dams. The jets can be divided into two categories of free jets and confined jets, caused by the distance from the discharge to limited boundaries points. The offset jet is a type of confined jet in which both free surface and wall boundaries are near the diffusion location. The jet flow due to the extreme curvature in the main flow path and the proximal portion of this flow with solid boundaries have characteristics that make it difficult to solve with simple turbulence models.

In this research, the offset jet phenomenon and related issues have been investigated. For this purpose, the offset jet flow pattern and probable factors in the complexity of this model have been simulated using Fluent software which analyses fluid flow in a two dimensional and three dimensional finite volume method. The simulation of offset jet flow pattern has been performed with a focus on investigating different models of turbulence k-ε, also boundary conditions, various wall functions and other effective coefficients in the numerical model and the model results compared with test case data findings and validating results, the necessary approaches in numerical simulation of this phenomenon for using in the next stages had been taken.

Keywords: k-ε; Turbulence; Offset Jet; Numerical Simulation.

1. Introduction

In the case of flow inlet with a relatively low thickness and high velocity in the lower velocity, the resulting field is called the jet. The jets are divided into two main categories including free jets and confined jets, by the distance of the discharge point to the limited boundaries [1]. The confined jets can be classified into three categories: impact jets that tend to the boundary direction, wall jets in which the flow is discharged to the boundary and offset jet.

The offset jet is a confined jet in which both of the free surface boundary and the horizontal wall parallel to the jet axis are located near the diffusion place and, depending on the boundaries distance to the gap, the jet extends toward the other boundary. In Figure 1, the characteristics of offset jets and its development stages are described [2].

The jet through a gap with the width w and the distance h from the wall, enters into the static fluid that surrounds it. Continuing the fluid flow, between the jet and the lower surface causes pressure decrease and jet extend to the wall until at the impingement point, finally the jet hits the wall and forms the converging zone. A portion of the inner shear layer of the fluid has been extended from the impingement point to the vortex zone influencing by pressure gradient and the flow is developed as wall jet at the distance far from the downstream of the gap. According to the above, the offset jet behavior in different areas after releasing is that in the orifice adjacent and at very short distance from the discharge

* Corresponding author: boroomand@tafreshu.ac.ir

http://dx.doi.org/10.28991/cej-2019-03091231

point, jet has free jet characteristics, in the zone around the impingement point (the impingement zone and a part of The pre- impingement zone) behaves like a reattachment jet, and in the zone away from diffusion place, the offset jet becomes the wall jet.

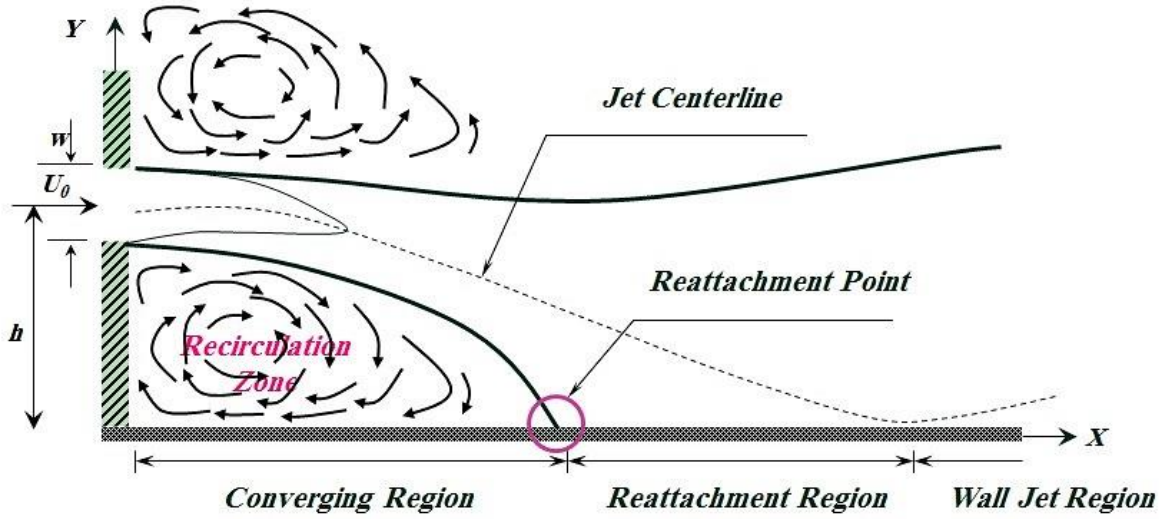

Figure 1. Schematic design of offset jet flow

Several studies have been carried out on the investigation of various offset jet parameters which have been often experimental due to the complicated mechanism of this flow. Following some of the studies are reviewed.

Bourque and Newman [3] and, Sawyer [4] studied the flow characteristics of offset jets adjacent the wall. The same work was done by McRee and Moses [5]. In the same year Perry [6], also studied the effect of the offset ratio and wall inclination angle on the impingement point. Rajaratnam and Subramanya [7], measured the wall static pressure and the average jet velocity in the converging zone and the wall jet zone, experimentally. Ayukawa and Shakouchi [8] investigated the effect of pressure oscillations on the velocity distribution in the converging zone experimentally. Johnston [9] based on the theory of the previous scientists, experimentally studied the offset jet and obtained the profile of flow and velocity for different depth waters. Nozaki et al. [10] obtained the results of experiments on the impingement point, the distribution of dynamic pressure on the wall, the jet centerline path and the damping of the maximum velocity of the jet axis in the converging zone. Hoch and Jiji [11] in 1981 investigated the jet path, the jet-to-wall impingement point, the wall pressure distribution, and damping of the maximum velocity of jet axis velocity, as well as the effect of the free secondary flow velocity on the impingement point. Salehi Neyshabouri [12], in a large study of offset jets in the University of Liverpool in 1988, conducted a numerical simulation of jets and determined their pattern.

Salehi Neyshabouri and Kamil Ali [13] studied the flow characteristics of two-dimensional offset jet experimentally. Kim et al. [14] investigated the characteristics of heat transfer and flow in near-wall offset jets. Song and Yon with a group of their colleagues [15], discussed the characteristics of heat transfer and flow in offset jets with the inclined wall using experimental methods and indicated the effect of the inclination angle on the impingement point and the maximum pressure point. Boroomand et al. [1] simulated the offset jet entering a domain with moveable bed using multiphase systems and their numerical results were verified by comparing the experimental data. Miozzi et al. [16] experimentally studied the effect of lateral wall placing at different distances from the jet outlet. Assoudi et al. [17] investigated the mean velocity and turbulence characteristics of the turbulent offset jet using a particle image velocimetry technique at three velocity ratios and for two offset ratios. Also, Assoudi et al. [18] experimentally and numerically investigated the flow field of variable density turbulent offset jet. They claimed that a good level of agreement was achieved, between the experiments and the calculations. Mohammadaliha and Farahanieh [19] focused attention on the influence of nozzle geometry on the evolution of a 3D incompressible turbulent offset jet. Their results imply that the spread rate, flow entrainment, and mixing rate of an offset jet issuing from a circular nozzle are lower than square-shaped one. Both and Szánthó [20] investigated an offset, attached jet both experimentally and numerically, applying the tangential room air distribution system. They applied three turbulence models for the 3D numerical simulation: standard, RNG k–ε and SST k–ω models and the conclusion was that the SST k–ω model seems to be the most accurate turbulence model.

The other factors, such as the flow line velocity, floatation (density variation), discharge direction, and the three dimensional effects, can further complicate the behavior of an offset jet.

When the discharged water density differs from the confined water density, a floating jet is formed and will be driven off upside or pushed down by buoyancy force. The behavior of a floating offset jet is determined by the buoyancy force, the boundaries, and also the layering. A better understanding of the flow behavior of an offset jet is very important in design experience.

When the impingement for more mixture is undesirable, calculating and designing methods for preventing from impingement should be applied, and vice versa, when the impingement is favorable, the relevant variables must be chosen and also the exact location of the impingement point should be determined. This last aspect is applicable to environmental discharges, such as urban and industrial wastewater conveyance, and the excessive heat discharge of power plants into large lakes or reservoirs. Researchers predicted the use of this discharge form to delay the rise of the jet by identifying the discharge location to the lower surface.

The whole mentioned subjects imply complicated and fully turbulent flow of offset jet that make a turbulent model choice, more significant.

A two-dimensional numerical simulation model that is expected to directly predict the offset jet flow field in relation to mixing interactions, recurrence patterns, continuous pressure and velocity distribution in a two-dimensional flow range, can eliminate experimental hypotheses and relationships in the previous works.

Also, a model for an unsteady flow may be useful for evaluating the establishment of a recurrence in the steady state. Unsteady simulations allow the designer to gain a more comprehensive look at the flow interactions and follow flow transmission from one to another during dynamic interactions.

This research includes theoretical and numerical study about jet - boundary reaction of a jet as parallel with the horizontal boundary and offset from a rigid vertical wall and the model results compared with test case data findings and validating results, the necessary approaches in numerical simulation of this phenomenon for using in the next stages had been taken:

- The jet is two-dimensional (planar), turbulent, submerged and non-floating.
- The received water is in the homogeneous density or temperature (inconsistent). The jet enters into a static waterbody.
- A two-dimensional model of Fluent software has been used to solve the turbulent field conditions including Standard, Realizable, and RNG.

Numerical simulations are used to conquest key interactions such as confined water flow direction, recurrence circulating, impingement at wall boundaries and wall jet flows. The results of the model are analyzed in relation to available laboratory data to determine the response of the complex jet-boundary and the offset jet behavior.

In all of this subjects, the turbulent term modeling had the main role, therefore in this research including turbulent model investigation, the available test case offset jet had been simulated by the most functional model of turbulence "k-ε model" in three states of Standard, RNG and Realizable, and the most suitable model to simulate this phenomenon will be presented by compared results.

The results of present work should help to better understand the physics and model the complicated offset flows and provide useful information in designing environmental water discharge.

2. Flow Equations

In the incompressible flow, the governing equations are expressed as following [21].

- Mass Conservation Equation (continuity equation)

$$\frac{\partial u_i}{\partial x_i} = 0 \tag{1}$$

- Momentum Conservation Equation (Navier-Stokes Equations)

$$\frac{\partial u_i}{\partial t} + u_j \frac{\partial u_i}{\partial x_j} = -\frac{1}{\rho}\frac{\partial p}{\partial x_i} + g_{xi} + \nu\nabla^2 u_i \tag{2}$$

In the above Equations, u_i is the instantaneous velocity component in the direction x_i; ν is the molecular viscosity; ρ is the fluid density; g_i is the gravity acceleration component in the direction i; P is the pressure term at each point of the fluid.

If it is possible to simulate irregular, instantaneous and random of the flow field quantities at any moment and at any point, then the equations above can be used in the numerical analysis of turbulent flow. If the instantaneous values of the velocity and pressure, or any other quantity as ϕ, can be separated into average and temporal values, then the following equations can be derived.

$$u_i = \overline{u_i} + u_i' \tag{3}$$

$$p = \overline{p} + p' \tag{4}$$

$$\phi = \overline{\phi} + \phi' \tag{5}$$

By replacing the above equations in continuity and momentum equations, there is no change in the continuity equation, but in the momentum equations the parameter $\overline{u_i' u_j'}$ is added.

- Continuity equation

$$\frac{\partial \overline{u_i}}{\partial x_i} = 0 \tag{6}$$

- Momentum equation

$$\frac{\partial \overline{u_i}}{\partial t} + \overline{u_j} \frac{\partial \overline{u_i}}{\partial x_j} = -\frac{1}{\rho} \frac{\partial \overline{p}}{\partial x_i} + g_{xi} + \frac{\partial}{\partial x_j} \left(\nu \frac{\partial \overline{u_i}}{\partial x_j} - \overline{u_i' u_j'} \right) \tag{7}$$

The parameter $\overline{\rho u_i' u_j'}$ is the Reynolds stress that imposes the effect of turbulent vortices in the fluid. In most turbulent flows, the Reynolds stress value is much greater than the stress caused by the molecular viscosity (ν ($\partial u_i / \partial x_j$)). To determine the Reynolds stress parameter, different turbulence models are used.

2.1. Turbulence Models

To solve turbulent flow field based on continuity equations and Reynolds, it is necessary to model Reynolds stresses in a special method. In the two-dimensional flow state, with three equations (one continuum and two momenta), the three unknown values of flow fields (velocities in directions x, y, and pressure) are determined. Disturbance terms in equations are assessed on the basis of a series of algebraic equations or differential equations [21].

Boussinesq (1877) assumed that turbulent stresses were proportional to the mean velocity gradient.

$$-\overline{u_i' u_j'} = \nu_t \left(\frac{\partial u_i}{\partial x_j} + \frac{\partial u_j}{\partial x_i} \right) - \frac{2}{3} k \delta_{ij} \tag{8}$$

$$\delta_{ij} = \begin{cases} 1 & i = j \\ 0 & i \neq j \end{cases} \tag{9}$$

ν_t is the eddy viscosity, unlike the molecular viscosity, is not a fluid property, but it is the function of the flow characteristics and its turbulence and varies from fluid to fluid and from point to point. Kronecker Delta δ_{ij} is used to apply the definition of eddy viscosity. The turbulence kinetic energy per unit mass (k) is expressed as follows:

$$k = \frac{1}{2} \left(\overline{u_i'}^2 + \overline{u_j'}^2 + \overline{u_k'}^2 \right) \tag{10}$$

The turbulent kinetic energy that provokes motion of fluid molecules and, while colliding with other molecules, makes changes in their momentums. Since the molecular viscosity is proportional to the mean velocity of free movement of the molecules, the eddy viscosity is also proportional to the velocity of oscillating motion and the sample length of the turbulent motion, which Prandtl in 1925 has introduced this length of the sample as the mixing length.

$$\nu_t \propto \overline{v} \cdot l \tag{11}$$

2.2. Types of Turbulence Models

Disturbance models are classified according to their design principles as well as the number of differential equations for the correlation of turbulent stresses with their mean velocity or gradients.

2.2.1. Zero Equations Models

In this model, no differential equation for disturbance quantities is presented. These models are relatively simple and experimental data in these models play an important role and turbulent stresses in each direction are proportional to the gradient velocity. Examples of these models are as follows:

- Constant Eddy Viscosity Model
- Mixing length model
- Prandtl's Free Shear Layer Model

2.2.2. One Equation Models

One equation models, unlike zero-equation models, use the equation for transferring quantity of turbulence. In fact, this equation is the relationship between the oscillatory velocity scale and the turbulence quantity, which is considered to be a turbulent kinematic energy square $\sqrt{k}$ as a velocity scale in turbulent motion and its value is calculated by the transport equation. The eddy viscosity is determined by the following equation.

$$\nu_t = c_\mu l\sqrt{k} \tag{12}$$

These models are better suited to high Reynolds flows, but they are unable to determine the viscous sublayer next to the wall. It is very difficult to detect longitudinal scale distribution in turbulent flows using these models.

In very complicated flows, it is difficult to specify the longitudinal scale distribution experimentally. Therefore, in order to increase the ability of turbulent models in this field, another differential equation is used to calculate the longitudinal scale. But most of the equations for the longitudinal scale are presented as combinations of k and l, that is, the second differential equation is shown in the form $z = k^{\alpha}.l^{\beta}$, and each of the forms of the equations for the longitudinal scale expresses a particular physical process. The general form of these equations is as follows:

$$\frac{\partial z}{\partial t} + u_i \frac{\partial z}{\partial x_i} = \frac{\partial}{\partial x_i}\left(\frac{\sqrt{k}}{\delta_z} + \frac{\partial z}{\partial x_i}\right) + C_{z1}\frac{z}{k}P_k - C_{z2}\frac{\sqrt{k}}{l} + S \tag{13}$$

Where, δ_z, C_{z1} and C_{z2} are experimental constants and P_k is kinetic energy generation that considers the reciprocative effects of Reynolds stresses and velocity gradients, and S is a source that varies according to the type of z. In free flows, the source term acts almost independently of the z type, and only near the wall the assumed z-gradient for diffusion indicates that the choice of $z = \varepsilon$ is better than other variables, in which case, in the equation ε, the secondary term S will be zero.

2.2.3. Two Equations Models

The most practical of two equations models is the k-ε model. Different forms of the k-ε model are presented, which will be explained in more detail, depending on the use of different forms of this model.

In high Reynolds numbers, the energy dissipation rate (ε) is equal to the molecular viscosity in the eddy fluctuations. The k-ε initial disturbance model was expressed by Kolmogorov and Pracking:

$$\frac{\partial k}{\partial t} + u_i \frac{\partial k}{\partial x_i} = \frac{\partial}{\partial x_i}\left(\frac{\nu_t}{\delta_k} + \frac{\partial k}{\partial x_i}\right) + \nu_t\left(\frac{\partial u_i}{\partial x_j} + \frac{\partial u_j}{\partial x_i}\right)\frac{\partial u_i}{\partial x_j} - \varepsilon \tag{14}$$

$$\frac{\partial \varepsilon}{\partial t} + u_i \frac{\partial \varepsilon}{\partial x_i} = \frac{\partial}{\partial x_i}\left(\frac{\nu_t}{\delta_\varepsilon} + \frac{\partial \varepsilon}{\partial x_i}\right) + c_{\varepsilon 1}\frac{\varepsilon}{k}P - c_{\varepsilon 2}\frac{\varepsilon^2}{k} \tag{15}$$

$$\nu_t = c_\mu \frac{k^2}{\varepsilon} \tag{16}$$

Lander and Spalding provided the constants of the above equations on the basis of experimental data according to Table 1.

Table 1. Lander and Spalding coefficient factors for k-ε equation

C_μ	$C_{\varepsilon 1}$	$C_{\varepsilon 2}$	δ_k	δ_ε
0.09	1.44	1.92	1.00	1.30

In the Fluent software, there are three types of k-ε equations:

1. Standard k-ε model

2. RNG k-ε model

3. Realizable k-ε model

The main difference between k-ε models as follows:

- The calculation method of the eddy viscosity μ_d;
- Prandtl turbulence numbers that govern the k and ε equations;
- Source and Sinks terms in the equation ε;

Standard k-ε model

In the standard k-ε model, which has the greatest application in turbulent flow analysis, Jones and Lander determined the constants of equations and also derived the equation. The standard model is used most frequently in high Reynolds numbers.

The standard k-ε model is a quasi-experimental method. The k equation in the model is precisely derived from the combination of Reynolds equations governing the flow. But the governing equation ε is based on experimental evidence and mathematical relations. In deriving these equations, it is assumed that the flow is fully turbulent and the molecular viscosity effect is negligible, and the equations governing this model are expressed by the following equations:

$$\rho\frac{dk}{dt}=\frac{\partial}{\partial x_i}\left[\left(\mu+\frac{\mu_t}{\delta_k}\right)\frac{\partial k}{\partial x_i}\right]+G_k+G_b-\rho\varepsilon \tag{17}$$

$$\rho\frac{d\varepsilon}{dt}=\frac{\partial}{\partial x_i}\left[\left(\mu+\frac{\mu_t}{\delta_\varepsilon}\right)\frac{\partial \varepsilon}{\partial x_i}\right]+C_{1\varepsilon}\frac{\varepsilon}{k}\left(G_k+C_{3\varepsilon}G_b\right)-C_{2\varepsilon}\rho\frac{\varepsilon^2}{k} \tag{18}$$

G_b and G_k are sources of equation k which have the buoyancy effect and gradient effect of mean velocity in the equation, and their equations are given as below. The following equation determines the eddy viscosity in the above equations.

$$\mu_t=\rho c_\mu\frac{k^2}{\varepsilon} \tag{19}$$

The constants of the above equation are in accordance with Table 2:

Table 2. Coefficient factors for Standard k-ε equation

C_μ	$C_{1\varepsilon}$	$C_{2\varepsilon}$	δ_k	δ_ε
0.09	1.44	1.92	1.00	1.30

δ_ε and δ_k are Prandtl numbers, and $C_{3\varepsilon}$ constant in equation ε is the effect of velocity in the direction of gravity and perpendicular to it.

$$C_{3\varepsilon}=\tanh\left|\frac{v}{u}\right| \tag{20}$$

Therefore, if the flow directions be in accordance with the direction of gravity and perpendicular to it, then in the shear layer, these constants are equal to 1 and zero, respectively.

2-2-3-2. RNG k-ε model

In this method, the turbulence of the flow is obtained on the basis of a precise statistical technique by mathematical relations. In fact, an additional term is introduced in equation ε, which increases the accuracy of the calculation in the strain rate flow. This model is more efficient than the standard k-ε model in circulating flows and, unlike the standard model, uses an analytical relation to determine the turbulent Prandtl numbers. Moreover, this model has a suitable

accuracy in the low Reynolds numbers. For this reason, this model is used more in curvature or geometric complexity fields to determine the turbulence quantities of the flow. The governing equations of this model are as follows:

$$\rho\frac{dk}{dt}=\frac{\partial}{\partial x_i}\left[\alpha_k\mu_{eff}\frac{\partial k}{\partial x_i}\right]+G_k+G_b-\rho\varepsilon \tag{21}$$

$$\rho\frac{d\varepsilon}{dt}=\frac{\partial}{\partial x_i}\left[\alpha_\varepsilon\mu_{eff}\frac{\partial \varepsilon}{\partial x_i}\right]+C_{1\varepsilon}\frac{\varepsilon}{k}\left(G_k+C_{3\varepsilon}G_b\right)-C_{2\varepsilon}\rho\frac{\varepsilon^2}{k}-R \tag{22}$$

The effective eddy viscosity μ_{eff} is determined by the following equations:

$$d\left(\frac{\rho^2 k}{\sqrt{\varepsilon\mu}}\right)=1.72\frac{\bar{\nu}}{\sqrt{\bar{\nu}^3-\left(1+C_\nu\right)}}d\bar{\nu} \tag{23}$$

$$\bar{\nu}=\frac{\mu_{eff}}{\mu} \tag{24}$$

Integrating above differential equation gains the eddy viscosity which is appeared to be a well-known relationship $\mu_t=\rho C_\mu\left(k^2/\varepsilon\right)$ in high values. Of course, in the low Reynolds values, especially near the wall, an initial differential state can be used.

The values of inverse turbulent Prandtl number, αk and αε, are determined by the following equation:

$$\left|\frac{\alpha-1.3929}{\alpha_0-1.3929}\right|^{0.6321}\left|\frac{\alpha+2.3929}{\alpha_0+2.3929}\right|^{0.3679}=\frac{\mu_{mol}}{\mu_{eff}} \tag{25}$$

In high Reynolds flows $\left(\mu_{mol}/\mu_{eff}\right)<<1$ with a fully turbulent flow, α_0 = 1.00, and the values of inverse turbulent Prandtl numbers will have constant values, i.e. $\alpha_k=\alpha_\varepsilon\approx1.393$.

The term R added to the equation ε in the RNG model rather than standard model corrects this model in zones with high strain rate and is defined in accordance with the following equation.

$$R=\frac{C_\mu\rho\eta^3\left(1-\eta/\eta_0\right)}{1+\beta\eta^3}\frac{\varepsilon^2}{k} \tag{26}$$

Where, $\eta\equiv Sk/\varepsilon$ and S represents the modulus of the mean rate-of-strain tensor, and is expressed by mean rate-of-strain:

$$S\equiv\sqrt{2S_{ij}^2}\quad,\quad S_{ij}=\frac{1}{2}\left(\frac{\partial u_i}{\partial x_j}+\frac{\partial u_j}{\partial x_i}\right) \tag{27}$$

In the above relations, the equations constants are as follows:

Table 3. Coefficient factors for k-ε RNG equation

C_μ	$C_{1\varepsilon}$	$C_{2\varepsilon}$	C_ν	η_0	β
0.0845	1.42	1.68	100	4.38	0.012

Realizable k-ε model

In this model, two major differences are found rather than the standard model in order to prevent the unbalance in the solution of equations, especially in the underlying layer of the boundary layer with high strain rate generation. These differences include:

1- Determination of the new equation of eddy viscosity μ_t;

2- Adding an additional source term to the equation ε that involves a large rotational variation.

This model has better results in flows with boundary layer, circulating flow, flow under inverse pressure gradient, flow

separation, planar and circular jets, and etc. compared to other commonly used k-ε models. The governing equations of this method are as follows.

The governing equation k is the standard model, but the governing equation ε is different:

$$\rho\frac{d\varepsilon}{dt}=\frac{\partial}{\partial x_i}\left[\left(\mu+\frac{\mu_t}{\delta_\varepsilon}\right)\frac{\partial\varepsilon}{\partial x_i}\right]+\rho C_1 S_\varepsilon-\rho C_2\frac{\varepsilon^2}{k+\sqrt{\nu\varepsilon}}-C_{1\varepsilon}\frac{\varepsilon}{k}C_{3\varepsilon}G_b \tag{28}$$

The eddy viscosity in the above equations is determined by the following equation so that the coefficient C_μ is not constant and is specified according to the relationships.

$$\mu_t=\rho c_\mu\frac{k^2}{\varepsilon} \tag{29}$$

$$C_\mu=1/\left(A_0+A_s\frac{u^* k}{\varepsilon}\right) \tag{30}$$

$$\begin{cases} u^*\equiv\sqrt{S_{ij}^2+\tilde{\Omega}_{ij}^2} \\ \tilde{\Omega}_{ij}=\Omega_{ij}-2\varepsilon_{ijk}\omega_k \\ \Omega_{ij}=\overline{\Omega}_{ij}-\varepsilon_{ijk}\omega_k \end{cases} \tag{31}$$

In the above equations, ω_k is the total amount of field rotation (angular velocity) and $\overline{\Omega}_{ij}$ represents the mean rate-of-rotation tensor.

$$\begin{cases} A_s=\sqrt{6}\cdot\cos\phi \\ \phi=(1/3)\cos^{-1}\left(\sqrt{6}\cdot W\right) \\ W=\dfrac{S_{ij}\cdot S_{jk}\cdot S_{ki}}{\tilde{S}} \end{cases} \tag{32}$$

S represents the modulus of the mean rate-of-strain tensor accordance with mean rate-of-strain as follows:

$$\begin{cases} S\equiv\sqrt{2S_{ij}^2} \\ S_{ij}=\dfrac{1}{2}\left(\dfrac{\partial u_i}{\partial x_j}+\dfrac{\partial u_j}{\partial x_i}\right) \end{cases} \tag{33}$$

The equations constants in this model are in accordance with Table 4.

Table 4. Coefficient factors for k-ε Realizable equation

C_1	$C_{1\varepsilon}$	$C_{2\varepsilon}$	δ_k	δ_ε	A_0
$Max\left[0.43,\dfrac{\eta}{\eta+5}\right]$	1.44	1.90	1.00	1.20	4.04

In order to compare, the constant coefficients of different k-ε models equations are presented in Table 1 below.

Table 5. Coefficient factors for k-ε equation

Coefficient factors						k-ε Models
$c_\mu=0.09$	$c_{1\varepsilon}=1.44$	$c_{2\varepsilon}=1.92$	$\delta_k=1.0$	$\delta_\varepsilon=1.30$		*Standard*
$c_\mu=0.0845$	$c_{1\varepsilon}=1.42$	$c_{2\varepsilon}=1.68$	$C_\nu=100$	$\eta_0=4.38$	$\beta=0.012$	RNG
$c_1=\mathrm{Max}[0.43,\dfrac{\eta}{\eta+5}]$	$c_{1\varepsilon}=1.44$	$c_{2\varepsilon}=1.90$	$\delta_k=1.0$	$\delta_\varepsilon=1.20$	$A_0=4.04$	Realizable

3. Materials and Methods

As mentioned, in this research, an experimental test case of this phenomenon, with accessible data, mentioned as follows, was simulated by a Fluent mathematical model to investigate the phenomenon of offset jet. The jet was entered into an aqueous environment and the jet centerline, the impingement point and the velocity profile will be investigated. In addition, different turbulent patterns (standard k-ε model, RNG k-ε model and realizable k-ε model), different wall functions and the effect of turbulent coefficients on problem parameters were among the cases in which more precise study conducted on them, and finally, the best method for simulating the offset jet flow pattern was extracted and the base of future modeling of this phenomenon will be provided.

3.1. Experimental Case Study

An available experimental case study is the results of Johnston's researches in Liverpool University. He provided a flume to do experiments which satisfied the following designing factors [11]:

Preparing sufficient and appropriate width and length for the channel in order to first create a 2-Dimensional jet and distract the effect of outlet condition of flow on the process of jet distribution in distribution place; applying methods with high sensitiveness to set the tailwater depth and inlet flow, supplying fixed head with entrance water to the system.

In all the experiments, the inlet flow was 3/33 m/sec, slot width was 0/014 m and the slot center was 0/35 m away from the bed.

3.2. Generated mesh

The choice of mesh dimensions is very important because by choosing large dimensions for the cells, the accuracy of the results will be reduced, and the inappropriate selection of small dimensions will also increase the discomfort of computational cost. Therefore, in order to select the dimensions, the sensitivity of the results to cell dimensions is required, and the mesh generation of the flow field based on the sensitivity analysis has been done.

Considering the flow conditions and the velocity gradients, the solution field was discretized by a suitable mesh. Significant areas were meshed with finer elements and using clustering intervals were covered, and finally a uniform mesh with an acceptable aspect ratio was generated. Figure 3 shows the generated quadrilateral mesh for this model. The number of nodes and element cells are 8349 and 8160, respectively.

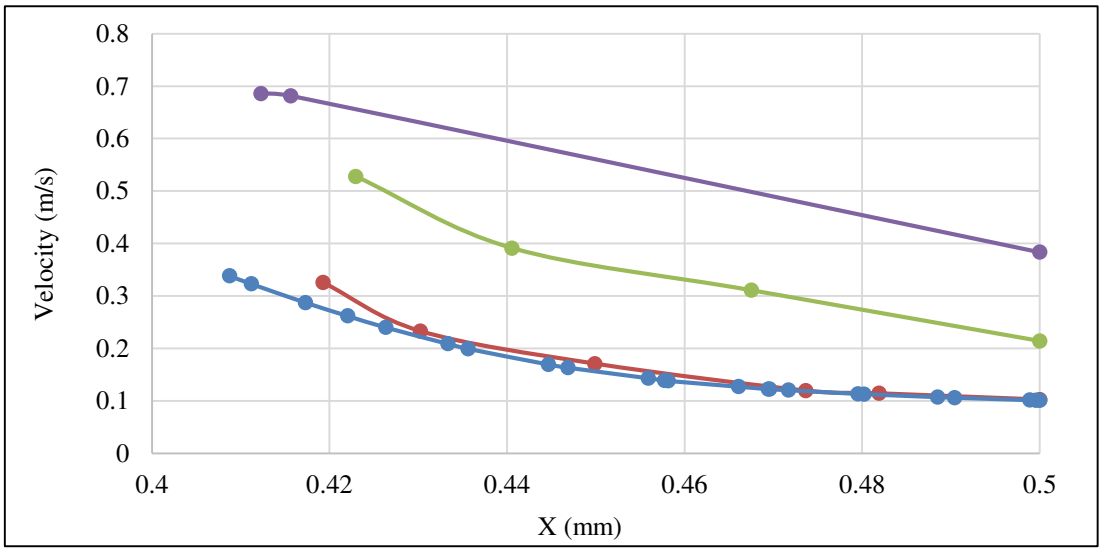

Figure 2. Mesh sensitivity analysis

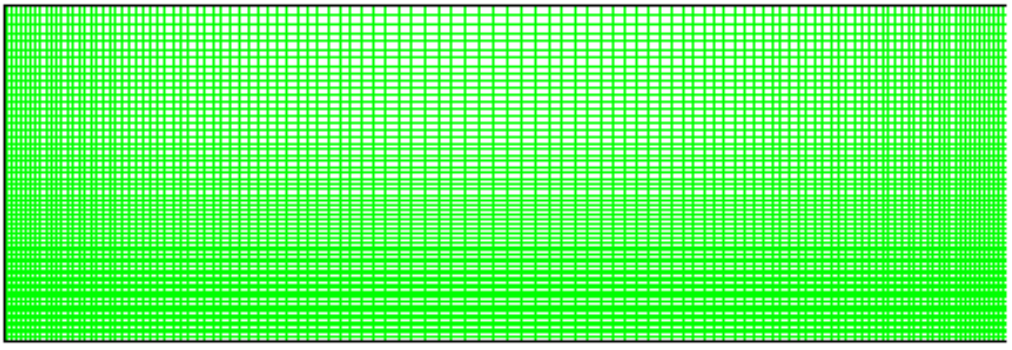

Figure 3. Generated mesh

As can be seen, the process of decreasing the dimensions of cells on the velocity values is significant, and then there is no significant change, and by increasing the size of the cells, only the computational cost will be increased

3.3. Boundary and initial conditions

Boundary conditions should be defined at all computational domain. Domain boundaries include:

- Input flow with a constant velocity of 3.33 m/sec and an opening rate of 0.014 m
- Output flow at the end of the flow field
- Upper and lower walls and elementary walls

The initial conditions of offset jet, a homogeneous, static and laminar water, was defined between the two horizontal rigid boundaries and a vertical rigid wall. It is worth mentioning that the boundary conditions and initial conditions were selected according to experimental data. Figure 3 indicates a schematic design of the solution field with boundary conditions.

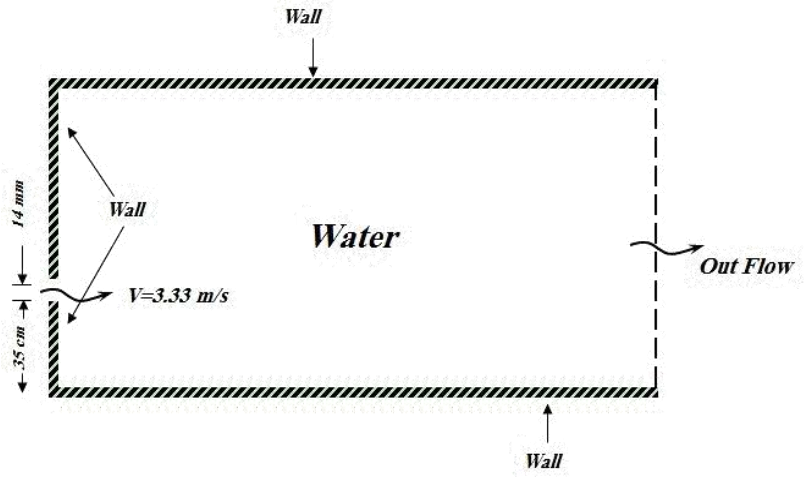

Figure 4. Schematic design of solution field

4. Results and Discussion

In order to solve, the model was implemented in the turbulent state with standard, RNG and realizable models, considering the conditions of offset jet phenomenon and applying suitable coefficients. The function of the standard wall and coefficients presented in tables related to these patterns was used to implement the model. The number of iterations had increased until the converging message was announced by the model Figure 5. The jet center line had been extracted of model results by a numerical code, in which the velocity amount had been obtained at every cell and then the maximum velocity situations indicate the jet centerline. The results are presented in Figures. 6 to 17. In the output figures of the models (6 to 12 and 14 to 16), the horizontal direction is the longitude axis of the jet flow direction and the transverse direction is the vertical wall of the jet entrance. In figures no. 9, 13, 17 and 21 the longitude and vertical axes are dimensionless by dividing the distance to the jet gap width (W).

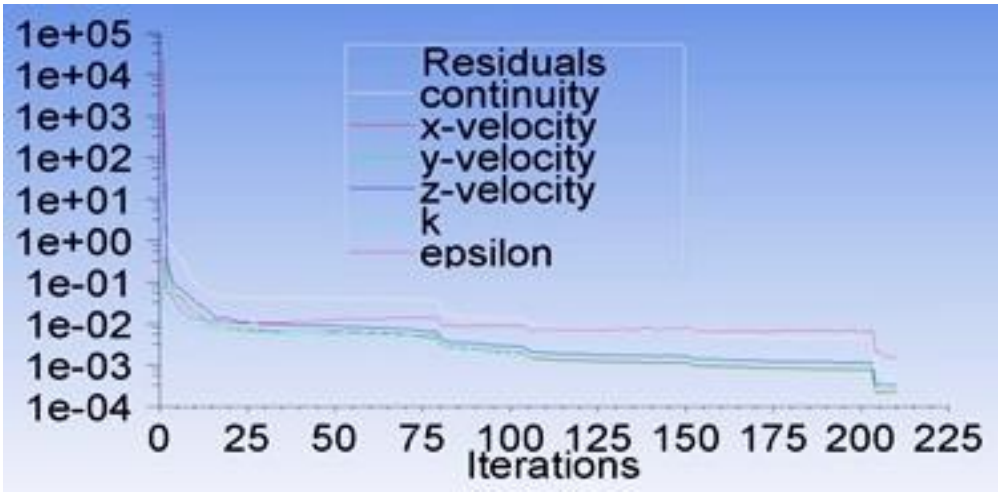

Figure 5. Residuals and iterations plot

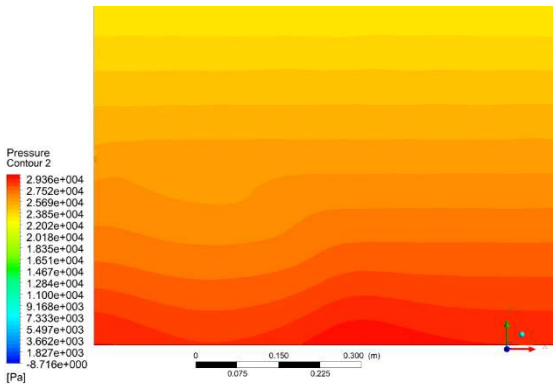

Figure 6. Pressure contours in k-ε Standard model

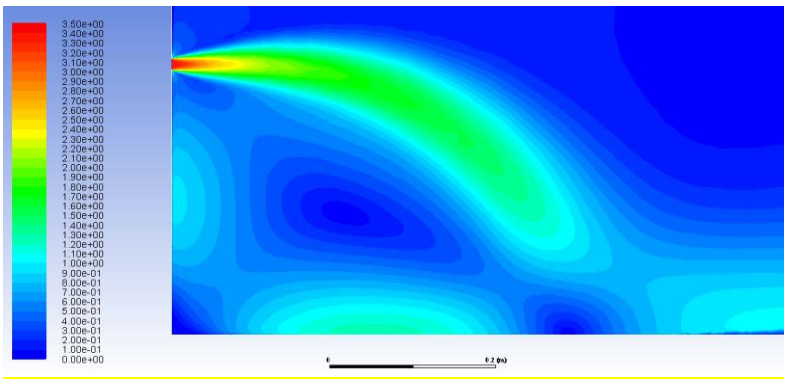

Figure 7. Velocity contours in k-ε Standard model (m/sec)

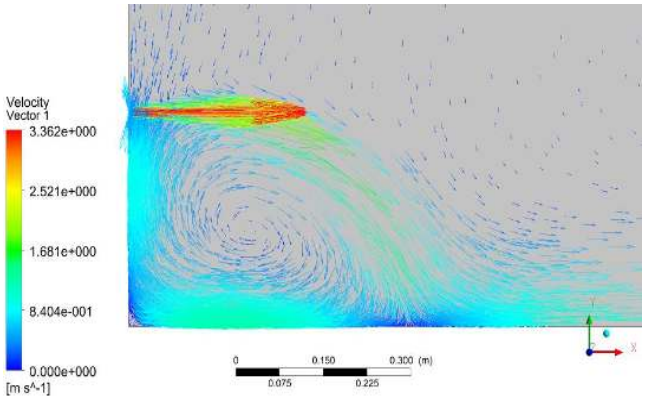

Figure 8. Velocity vectors in k-ε Standard model

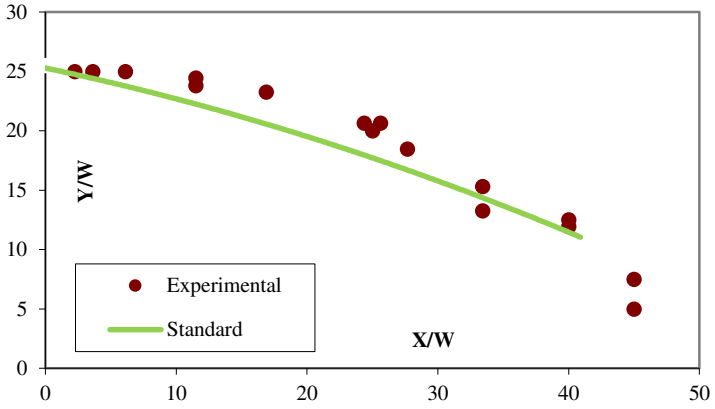

Figure 9. Comparison between numerical simulation and experimental data to prediction about jet center line in k-ε Standard model

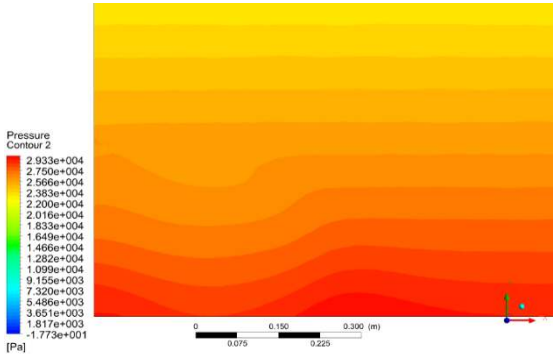

Figure 10. Pressure contours in k-ε RNG model

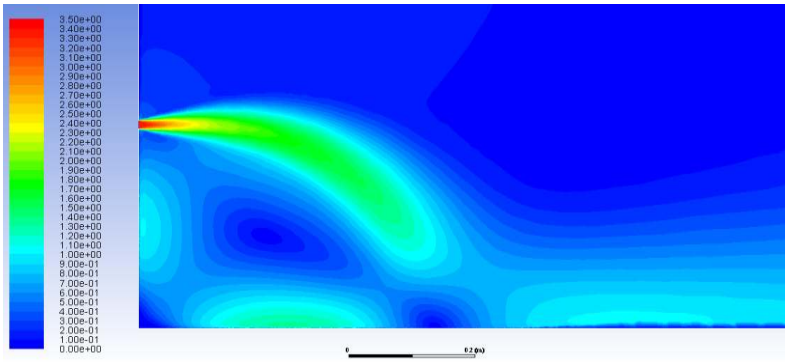

Figure 11. Velocity contours in k-ε RNG model (m/sec)

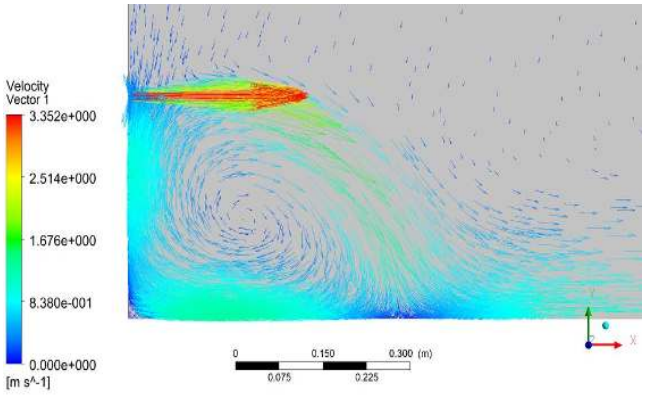

Figure 12. Velocity vectors in k-ε RNG model

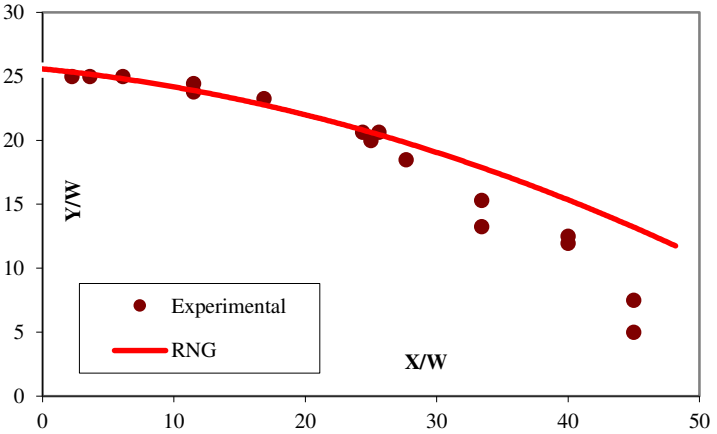

Figure 13. Comparison between numerical simulation and experimental data to prediction about jet center line in k-ε RNG model

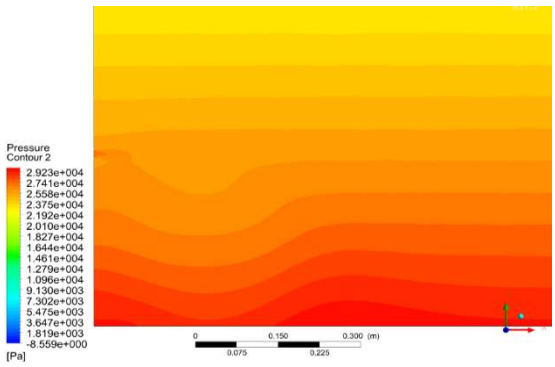

Figure 14. Pressure contours in k-ε Realizable model

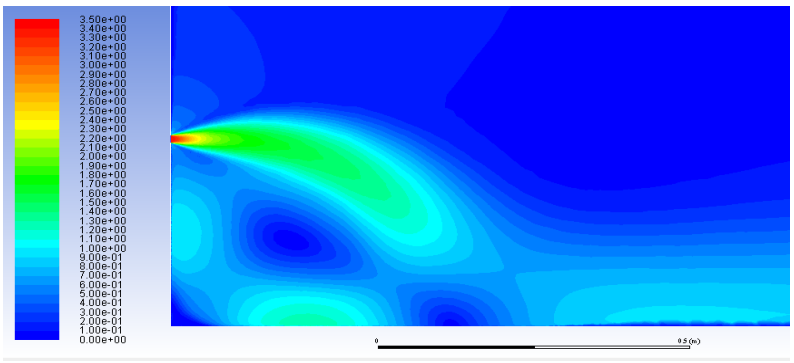

Figure 15. Velocity contours in k-ε Realizable model (m/sec)

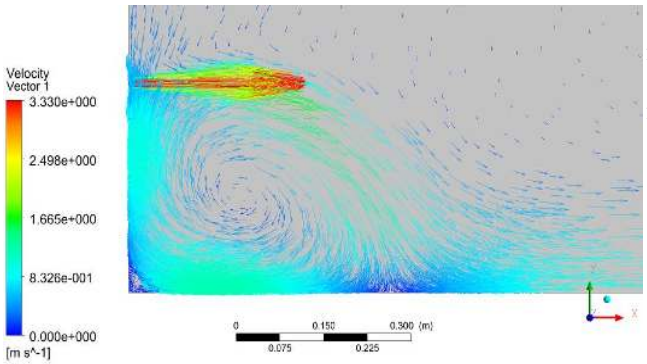

Figure 16. Velocity vectors in k-ε Realizable model

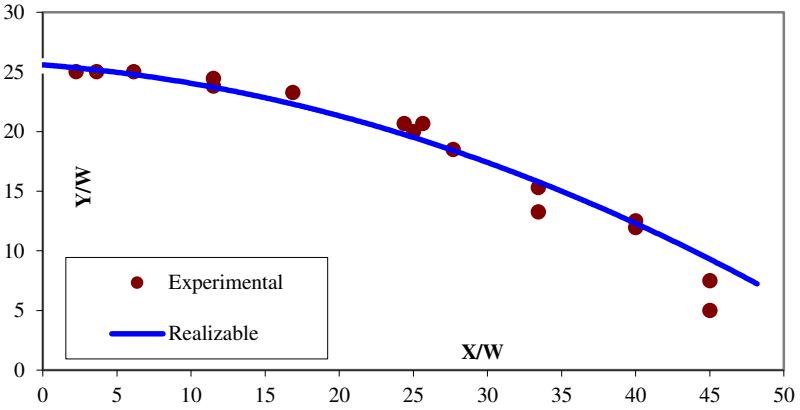

Figure 17. Comparison between numerical simulation and experimental data to prediction about jet center line in k-ε Realizable model

It is worth noting that in all models for velocity and pressure coupling, the SIMPLE model was used. The effect of under-relaxation factor on the performance of models was observed and the results were presented in the most appropriate under-relaxation factor. Using the above results and sureness of better efficiency of a turbulent Realizable model, the other results will be precisely investigated. It is worth mentioning that the above results had been obtained on the basis of velocity term and in this section, the results obtained from the pressure term are considered.

As been seen in result section, generally the pressure contour for all of three states including Standard, RNG and Realizable appear similar, so that the pressure profile for whole three states has been extracted and compared to each other at three different depths.

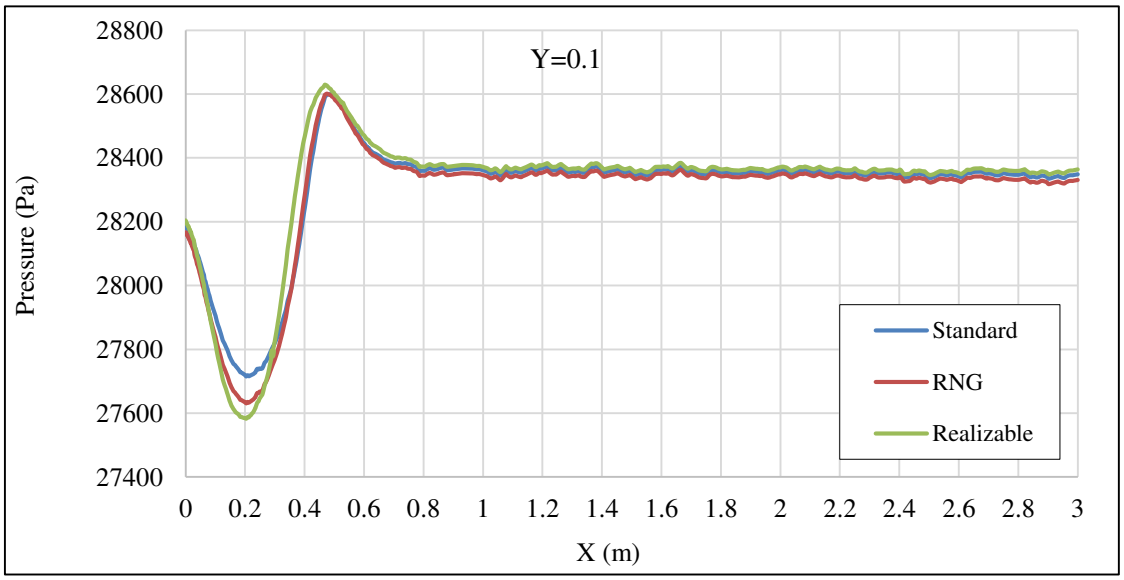

Figure 18. Pressure profile for y= 0.1 in different states of k-ε model

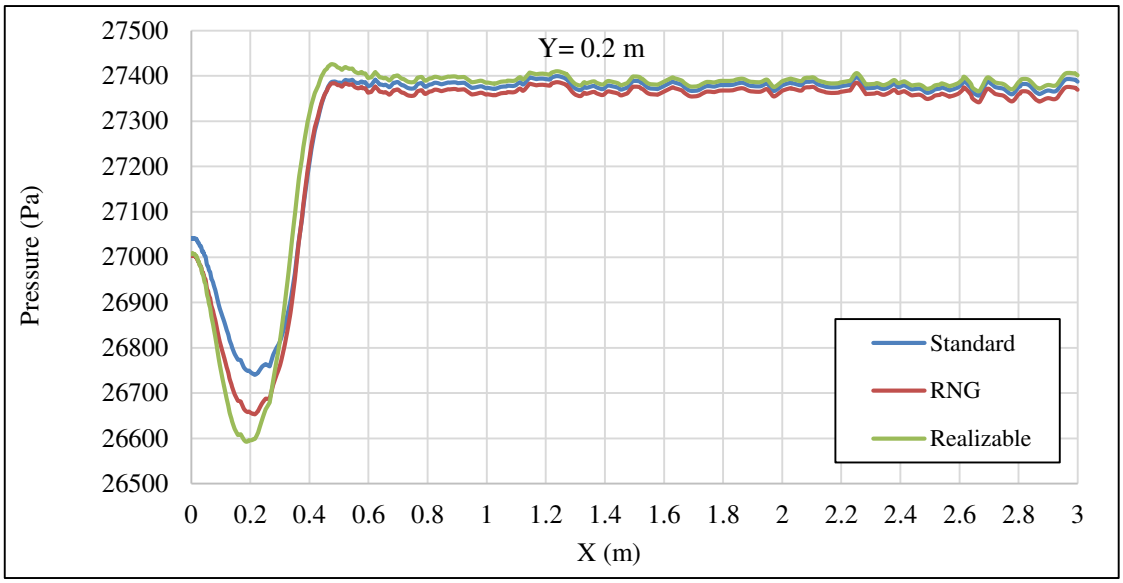

Figure 19. Pressure profile for y= 0.2 in different states of k-ε model

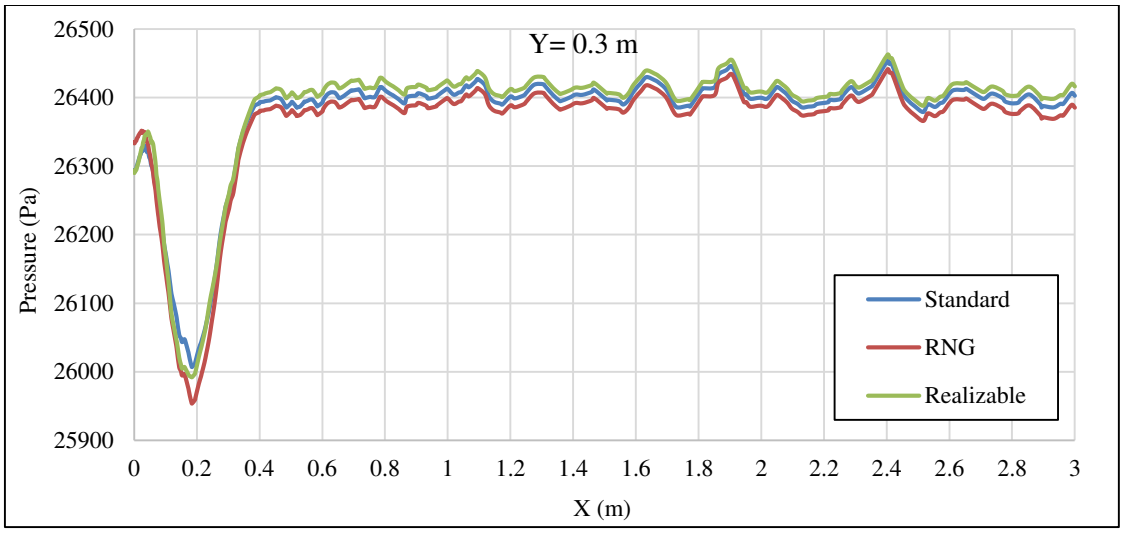

Figure 20. Pressure profile for y= 0.3 in different states of k-ε model

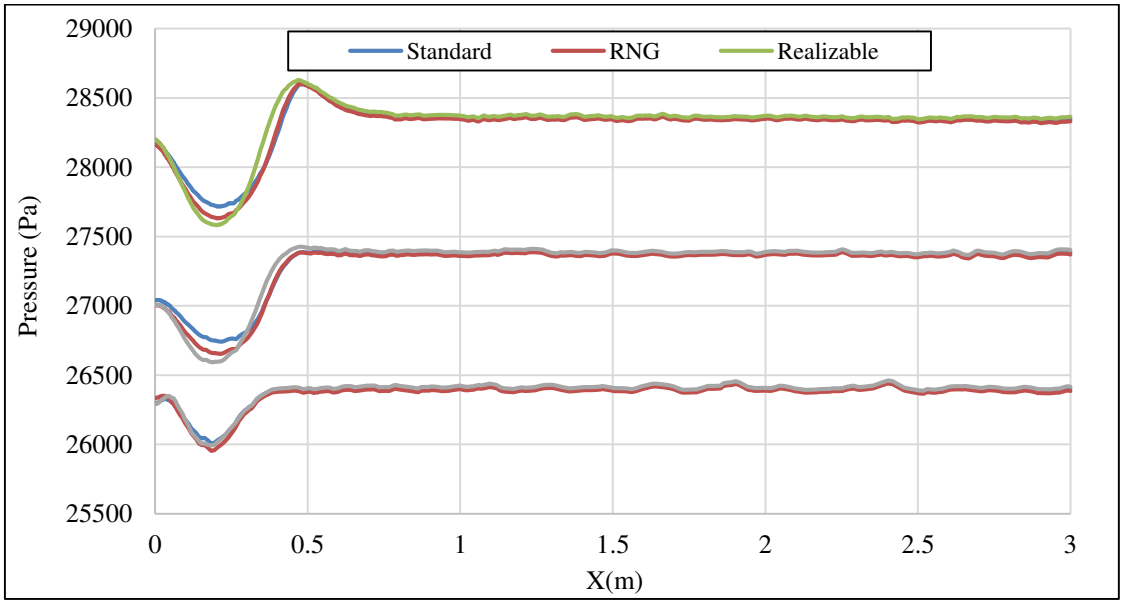

Figure 21. Pressure profile for three depths in different states of k-ε model

As been seen, the Realizable model indicates less pressure at recirculation zone for all three depths, considering the adaptation of this model velocity results and measured data, the conclusion is that the pressure pattern presented by this model, should be adapted more to reality and the pressure pattern at the offset jet recirculation zone will be obtained when measured data is not available. Also increasing the pressure oscillation from y=0.1 to y=0.3 at further distances from the jet entrance is noticeable.

5. Conclusion

The jet center line is presented in order to better comparison of the results collectively. Figure 22.

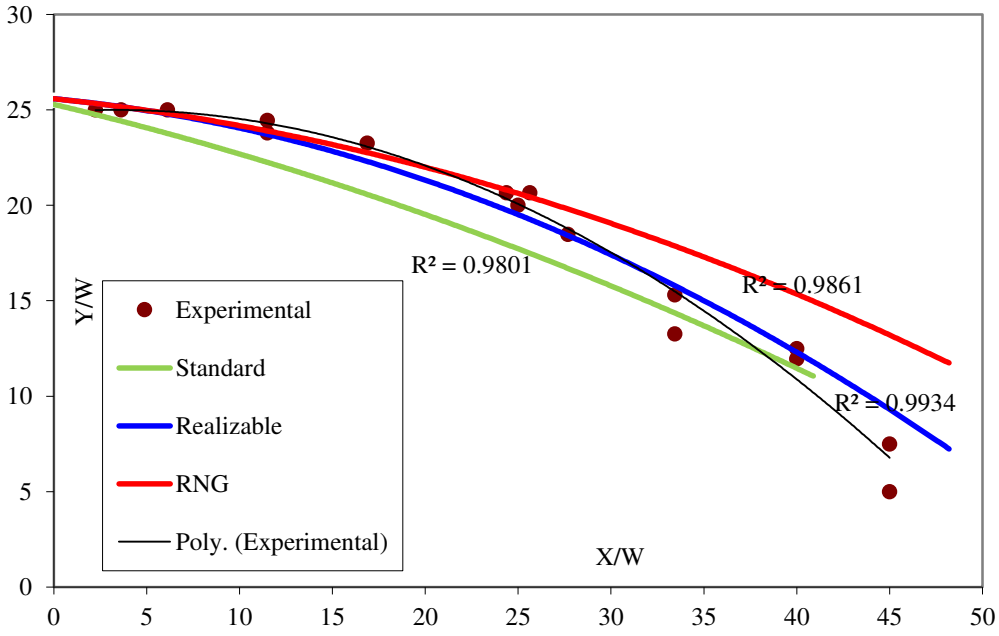

Figure 22. Comparison between numerical simulation and experimental data to prediction about jet center line in different states of k-ε model

As can be seen:

- The realizable turbulent model predicts the offset jet centerline path better than the other models.
- Predictions of the turbulent Standard model on the inlet are underestimated and the jet path in the initial distances is lower than the experimental results.
- The RNG turbulent model overestimates impingement zone and prediction the jet center line path rather than experimental results.
- If the difference of R^2 from the unit value for each model is the base of the error of each model, then the error of each model is as follows:

Standard	**2 %**
RNG	**1.4 %**
Realizable	**0.6 %**

In sum, the realizable turbulent model is more suitable for offset jet modeling and can be used in related designs. This turbulent model can be utilized in all future offset jet modeling. The effect of different wall functions (standard and unbalanced wall functions) is intangible in the results. It seems that according to the flow pattern of this phenomenon, such a conclusion is possible.

6. Conflict of Interest

The authors declare no conflict of interest.

7. References

[1] M.R. Boroomand, A. A. Salehi-Neyshaboury, K. Aghajanloo. "Numerical Simulation of Sediment Transport and Scouring by an Offset Jet" Canadian Journal of Civil Eng 34 (2007) 1267-1275. doi: 10.1139/l07-050.

[2] A. Nasr, J. Lai, "A Turbulent Plane Offset Jet with Small Offset Ratio" Experiments in Fluids 24 (1998) 47–57. doi: 10.1007/s003480050149.

[3] C. Bourque, B. G. Newman, "Reattachment of a Tow-Dimensional Incompressible Jet to an Adjacent Flat Plate" Aeronautical Quarterly 11 (2016) 201-232.doi: 10.1017/s0001925900001797.

[4] R. A. Sawyer, "The Flow Due to a 2D Jet Issuing Parallel to a Flat Plate" Journal of Fluid Mechanic 9 (1960) 543-561.doi: 10.1017/s0022112060001304.

[5] D. I. McRee, H. I. Moses, "The Effect of Aspect Ratio and Offset Ratio on Nozzle Flow and Jet Reattachment" Advances in Fluids, ASME Press, New York, 1967, pp. 142-161.

[6] C. C. Perry, "Two-Dimensional Jet Reattachment" PhD thesis, University of Michigan, Michigan, 1967.

[7] N. Rajaratnam, N. Subramanya, "Plane Turbulent Reattachment Wall Jet" Journal of Hydraulic Division, 1968, (94) 95-112.

[8] K. Ayukawa, T. Shakouchi. "Analysis of a Jet Attaching to an Offset Parallel Plate" Bulletin of the JSME 19 (130) 395-401.doi: 10.1299/jsme1958.19.395.

[9] A. J. Johnston, "Experimental Study of Shallow Submerged Turbulent Jets", Ph. D Thesis, University of Liverpool, Liverpool, 1978.

[10] T. Nozaki, K. Hatta, N. Satu, H. Matsumua, "Reattachment Flow Issuing From a Finite Nozzle" Bulletin of The JSME 24 (1981) 363-369.doi: 10.1299/jsme1958.24.363.

[11] J. Hoch, M. Jiji, "Tow-Dimensional Turbulent Offset Jet Boundary Interaction", Transactions of The ASME, Journal of Fluids Engineering 103 (1981) 154-161.doi: 10.1115/1.3240766.

[12] A. A. Salehi Neyshabouri, "Impingement of Offset Jets on Rigid and Movable Beds" Ph. D Thesis, University of Liverpool, Liverpool, 1988.

[13] A. A. Salehi Neyshabouri, K. H. M. Ali, "Flow Field of an Offset Jet" Proceedings of the International Conference on Physical Modeling of Transport and Dispersion, Massachusetts, Cambridge University Press , 1990, pp.13-18.

[14] D. S. Kim, S. H. Yoon, D. H. Lee, K. CH. Kim, "Flow and Heat Transfer Measurements of a Wall Attaching Offset Jet" International Journal of Heat Mass Transfer 39 (1996) 2910-2913.doi: 10.1016/j.ijheatmasstransfer.2014.07.008.

[15] H. B. Song, S. H. Yoon, D. H. Lee, "Flow and Heat Transfer Characteristics of a Two-Dimensional Oblique Wall Attaching Offset Jet" International Journal of Heat and Mass Transfer 43 (2000) 2395-2404.doi: 10.1016/s0017-9310(99)00312-9.

[16] M. Miozzi, F. Lalli, G. P. Romano, "Experimental investigation of a free-surface turbulent jet with Coanda effect" Experiments in Fluids 49 (2010) 341-353.doi: 10.1007/s00348-010-0885-1.

[17] Ali Assoudi, A., S. Habli, N. M. Saïd , H. Bournot, and G. Le Palec, "Experimental and numerical study of an offset jet with different velocity and offset ratios", Engineering Applications of Computational Fluid Mechanics (2015): 490–512.doi: 10.1080/19942060.2015.1071525

[18] Ali Assoudi, A., S. Habli, N. M. Saïd , H. Bournot, and G. Le Palec, "Three-dimensional study of turbulent flow characteristics of an offset plane jet with variable density", International Journal of Heat and Mass Transfer 52 (2016) 2327–2343.doi: 10.1007/s00231-015-1750-9.

[19] Mohammadaliha, N., H. Afshin, and B. Farahanieh, "Numerical Investigation of Nozzle Geometry Effect onTurbulent 3-D Water Offset Jet Flows" Journal of Applied Fluid Mechanics 9 (2016): 2083-2095. doi: 10.18869/acadpub.jafm.68.235.21386.

[20] Balázs, B., and Z. Szánthó, , "Experimental and Numerical Investigation of an Offset Jet Using Tangential Air Distribution System", Periodica Polytechnica Mechanical Engineering (2016): 129–136.doi: 10.3311/PPme.8017.

[21] Wu W., Rodi W., Wenka T., "3D Numerical Modeling of Flow And Sediment Transport In Open Channel" Journal of Hydraulic Engineering, Vol. 126, No. 1, 2000.doi: 10.1061/(asce)0733-9429(2000)126:1(4).